

INTEGRAL observations of SS433: system’s parameters and nutation of supercritical accretion disk

A.M. Cherepashchuk¹, R.A. Sunyaev², S.V. Molkov², E.A. Antokhina¹,
K.A. Postnov¹, A.I. Bogomazov¹ *

¹*Moscow M.V. Lomonosov State University, Sternberg Astronomical Institute, Universitetskij pr. 13, Moscow 119992, Russia*

²*Space Research Institute, Moscow, Russia*

Accepted Received; in original form

ABSTRACT

Based on multiyear *INTEGRAL* observations of SS433 in 2003–2011, a composite IBIS/ISGRI 18–60 keV orbital light curve is constructed around zero precessional phases $\psi_{pr} = 0$ at the maximum accretion disk opening angle. It shows a peculiar shape with significant excess near the orbital phase $\phi_{orb} = 0.25$, which is not seen in the softer 2–10 keV energy band. The 40–60 keV orbital light curve demonstrates two almost equal humps at phases ~ 0.25 and ~ 0.75 , most likely due to nutation effects of the accretion disk. The nutational variability of SS433 in 15–50 keV with a period of $\simeq 6^d.290$ is independently found from analysis of *Swift*/*BAT* data. The change of the off-eclipse 18–60 keV X-ray flux with the precessional phase shows a double-wave form with strong primary maximum at $\psi_{pr} = 0$ and weak but significant secondary maximum at $\psi_{pr} = 0.6$. A weak variability of the 18–60 keV flux in the middle of the orbital eclipse correlated with the disk precessional phase is also observed. The joint analysis of the broadband 18–60 keV orbital and precessional light curves confirms the presence of a hot extended corona in the central parts of the supercritical accretion disk and constrains the binary mass ratio in SS433 in the range $0.5 \gtrsim q \gtrsim 0.3$, suggesting the black hole nature of the compact object.

Key words: X-rays: binaries — Stars: individual: SS433 — black hole physics

* E-mail: cherepashchuk@gmail.com(AMCh); kpostnov@gmail.com(KAP);elant@sai.msu.ru(EAA)

1 INTRODUCTION

SS433 is a unique galactic steadily superaccreting microquasar with mildly relativistic ($v = 0.26c$), precessing jets located at a distance of 5.5 kpc (Margon 1984; Cherepashchuk 1981, 1989; Fabrika 2004). The system exhibits three photometric and spectral periodicities related to precession ($P_{\text{pr}} \simeq 162^d.5$), orbital ($P_{\text{orb}} \simeq 13^d.082$) and nutation ($P_{\text{nut}} \simeq 6^d.29$) periods (Goranskij et al. 1998), which are found to be stable during an observational period of more than 30 years (Davydov et al. 2008). Despite the wealth of observations, the nature of the compact star in SS433 remains inconclusive. The presence of absorption lines in the optical spectrum of the companion (Gies et al. 2002b; Hillwig & Gies 2008) suggests its spectral classification as \sim A7Ib supergiant. Assuming these lines to be produced in the optical star photosphere, their observed orbital Doppler shifts would correspond to the mass ratio of compact (M_x) and optical (M_v) star $q = M_x/M_v \sim 0.3 \pm 0.11$ and masses $M_x = (4.3 \pm 0.8)M_\odot$, $M_v = (12.3 \pm 3.3)M_\odot$, respectively, pointing to the black hole nature of the compact star.

Modeling of all *INTEGRAL* eclipses of the source available before 2010 using a purely geometrical model yielded independent constraints on the binary mass ratio $q = 0.25 - 0.5$ with the most probable value $q = 0.3$, suggesting the mass of the compact companion $M_x \simeq 5.3M_\odot$ and the optical star $M_v \simeq 17.7M_\odot$ for the observed optical star mass function $f_v = 0.268M_\odot$ (Cherepashchuk et al. 2009, 2012). This firmly places SS433 among black-hole high-mass X-ray binaries (HXMB). Thus SS433 can be the only known example of galactic HMXB at an advanced evolutionary stage (Cherepashchuk 1981, 1989) with supercritical accretion (Shakura & Sunyaev 1973) onto a black hole. Its study in different spectral bands provides invaluable information for theory of evolution of binary star and the formation of relativistic jets. However, adopting the spectral classification A7Ib does not rule out the presence of neutron star in SS433 (Goranskij 2011). Preliminary analysis of the new optical spectroscopic observations by SS433 on large telescopes may raise doubts on the correctness of the spectral classification of the optical star, which apparently relates to a very powerful mass loss from the optical star and the accretion disk in this system. Clearly, new observations of SS433 and independent determination of the binary system parameters are needed.

The basic picture of hard X-ray emitting regions, as emerged from analysis of X-ray data (Antokhina et al. 1992; Fabrika 2004; Filippova et al. 2006; Cherepashchuk et al. 2003,

2005, 2009; Krivosheyev et al. 2009), includes hot X-ray jet propagating through a funnel in the supercritical accretion disk, filled with hot scattering medium (a corona). The X-ray spectrum of SS433 in the 3-100 keV range can be fitted by two-component model (thermal X-ray emission from the jet and thermal comptonization spectrum from corona) elaborated in (Krivosheyev et al. 2009). The scattering corona parameters are: $T_{cor} \simeq 20$ keV, Thomson optical depth $\tau_T \simeq 0.2$ and mass outflow rate in the jet $\dot{M}_j = 3 \times 10^{19}$ g/s. This parameters suggest the coronal electron number density around 5×10^{12} cm⁻³, which is typical in the wind outflowing with a velocity of $v \sim 3000$ km/s from a supercritical accretion disk with mass accretion rate onto the compact star $\dot{M} \sim 10^{-4}$ M_⊙/yr at distances $\sim 10^{12}$ cm from the center, where a Compton-thick photosphere is formed (Fabrika 2004). The size of the disk photosphere was independently estimated from measurements of fast optical aperiodic variability (Burenin et al. 2010).

Here we analyze hard X-ray eclipses of SS433 near moment T3, corresponding to maximum separation of the moving emission lines from jets and the maximum opening angle of the accretion disk, in combination with the precessional variability as observed by *INTEGRAL* in 2003-2011, and treat them in terms of our multicomponent geometrical model (Cherepashchuk et al. 2009). In addition to precessional and orbital hard X-ray variability, which allowed us to constrain the parameters of the system within the adopted geometrical model (Cherepashchuk et al. 2009), here we focus on the features in the observed hard X-ray light curve which can be interpreted in terms of nutation of the supercritical accretion disk in SS433 (Cherepashchuk et al. 2012).

In Section 2 we describe *INTEGRAL* observations used for the analysis. In Section 3 we discuss the precessional variability of SS433. In Section 3.1 we study the primary eclipse of SS433 in hard X-rays and present IBIS/ISGRI spectra of SS433 obtained at different orbital phases. In Section 4 we consider evidence for nutational variability of SS433 from *Swift*/BAT and *INTEGRAL* observations. We discuss the results in Section 6 and summarize our findings in Section 7.

2 OBSERVATIONS

Dedicated *INTEGRAL* observations of hard X-ray eclipse are summarized in Table 1. **The observations have been carried out using 5×5 dithering mode, so only IBIS/ISGRI data have been analyzed.** The observations were mostly concentrated around preces-

Table 1. Dedicated *INTEGRAL* observations of SS433 primary eclipses at precessional phases with maximum accretion disk opening

Set	<i>INTEGRAL</i> orbits	Dates	Precessional phase ψ_{pr}
I	67-70	May 2003	0.001-0.060
II	555-556	May 2007	0.980-0.014
III	608-609	October 2007	0.956-0.990
IV	612-613	October 2007	0.030-0.064
V	722-723	September 2008	0.057-0.091
VI	984	November 2010	0.870-0.890
	987	November 2010	0.930-0.940
VII	1040-1041	April 2011	0.910-0.950

sional phase zero ('the T3 moment' in terms of the kinematic model of SS433 (Cherepashchuk 1981)), where the accretion disk is maximum opened to the observer and the non-eclipsed X-ray flux from the source is the highest, reaching typically ~ 20 mCrab in the 20-60 keV band.

The *INTEGRAL* data were processed using the original software package elaborated by the IKI *INTEGRAL* team for the IBIS/ISGRI telescope image reconstruction (see (Molkov et al. 2004; Revnivtsev et al. 2004b; Krivonos et al. 2010) for more detail). The 18-60 keV light curves of SS433 eclipses obtained in observations I-VII near precession phase zero (moment T3), from Table 1 are presented in Fig. 1.

3 PRECESSIONAL VARIABILITY

We start with producing the observed precessional light curve of SS433 from all available *INTEGRAL* data taken outside the primary eclipses. For the analysis of precessional variability of SS433 we have used both data from our *INTEGRAL* observing program of SS433 and publically available data of all *INTEGRAL* observations where the source fell in the field of view of the IBIS/ISGRI telescope (< 13 degrees). The total exposure time of the selected data is approximately 8.5 Ms. To perform precessional-phase-resolved analysis we ascribed to each SCW (Science Window or SCW, the natural piece of the *INTEGRAL* data – pointing observation with an exposure time of $\sim 2 - 5$ ks) the appropriate orbital and precessional phases. The phases have been calculated using the ephemeris from (Fabrika 2004):

the orbital primary minimum (corresponding to $\phi_{orb} = 0$, when the optical star is in front of the disk)

$$JD_{MinI}(\text{hel}) = 2450023.62 + 13.08211 \times E,$$

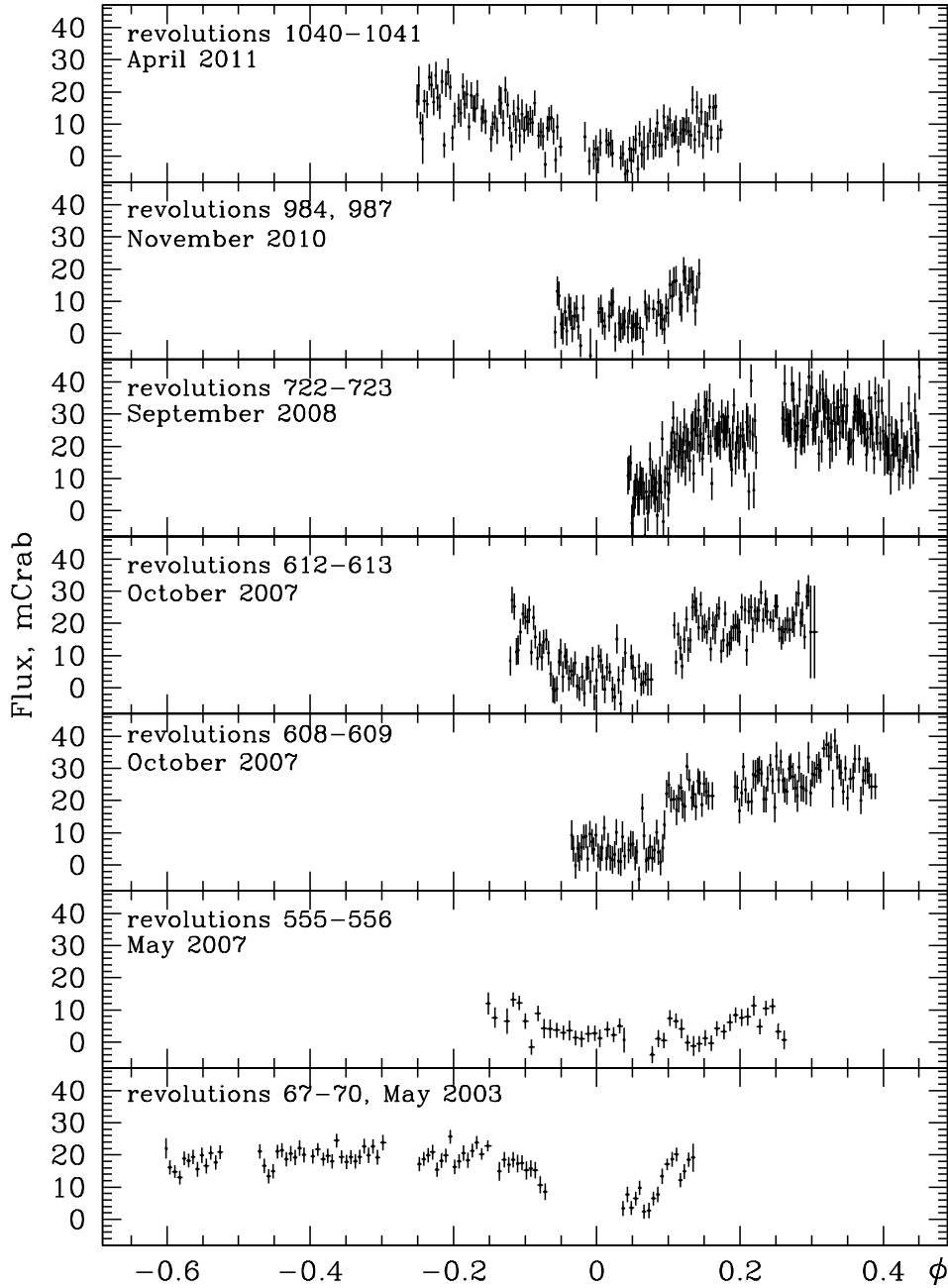


Figure 1. Primary eclipses of SS433 near precession phase zero observed by *INTEGRAL* (observations I-VII from Table 1). 18-60 keV IBIS/ISGRI fluxes obtained in individual science windows are shown.

the zero precession phase (corresponding to the T3 moment, $\psi_{pr} = 0$, when the disk is maximum open to the observer)

$$JD_{T3}(\text{hel}) = 2443507.47 + 162.375 \times E1.$$

At a distance of 5.5 kpc to SS433, as derived from the kinematic properties of moving emission lines (Fabrika 2004), the observed 18-60 keV X-ray flux corresponds to a maximum uneclipsed hard X-ray luminosity of 3×10^{35} erg/s. The precessional change of the X-ray flux

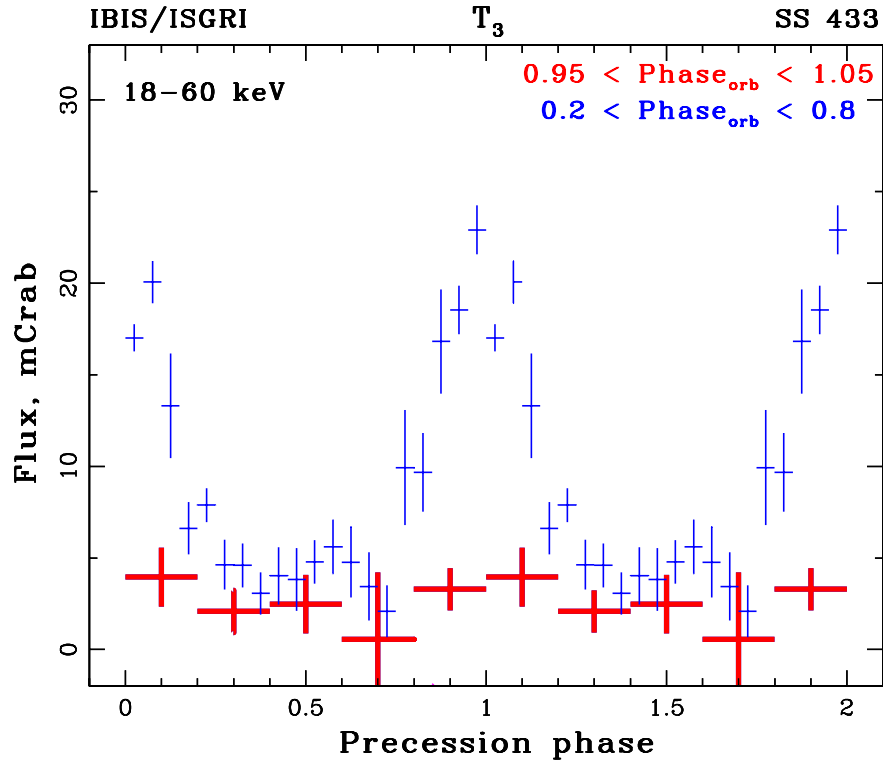


Figure 2. Precessional 18-60 keV light curves out of the primary orbital eclipses (upper thin crosses) and inside the eclipses (thick gray crosses)

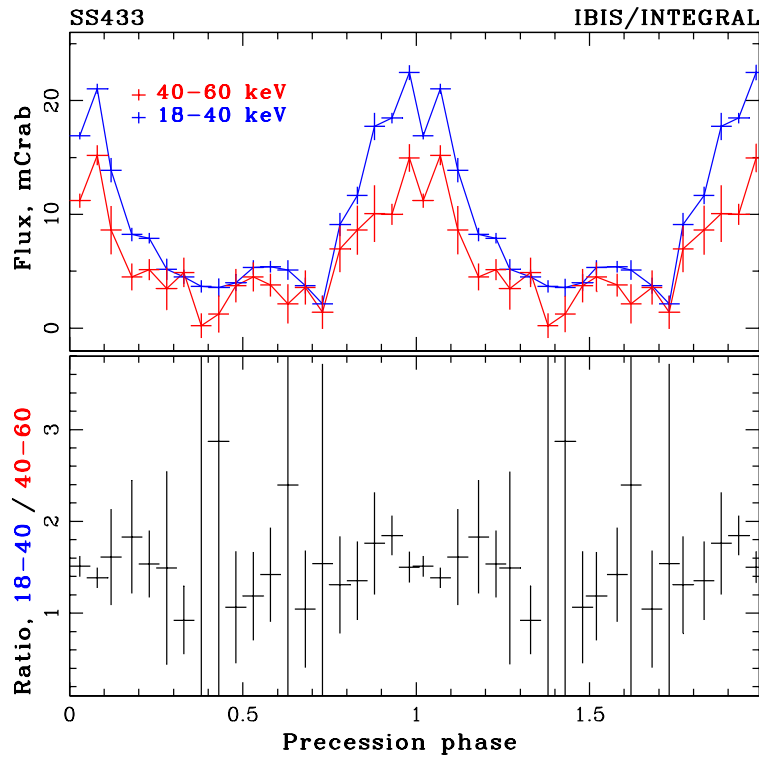


Figure 3. Precessional 18-40/40-60 keV light curves (upper panel) and the hardness ratio (bottom panel). Orbital eclipses are excluded.

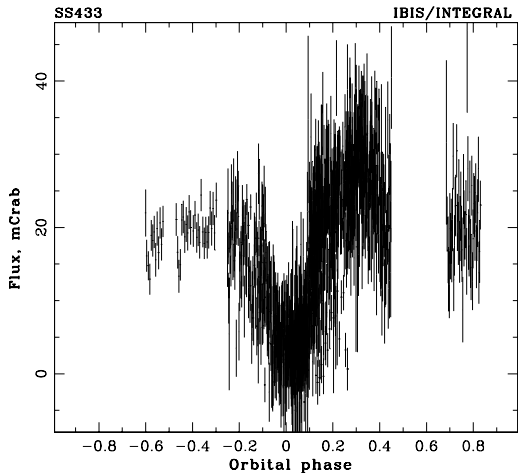


Figure 4. Composite IBIS/ISGRI 18-60 keV X-ray eclipse light curve around precessional phase zero ($0.08 < \psi_{pr} < 1.2$) for observations in Table 1.

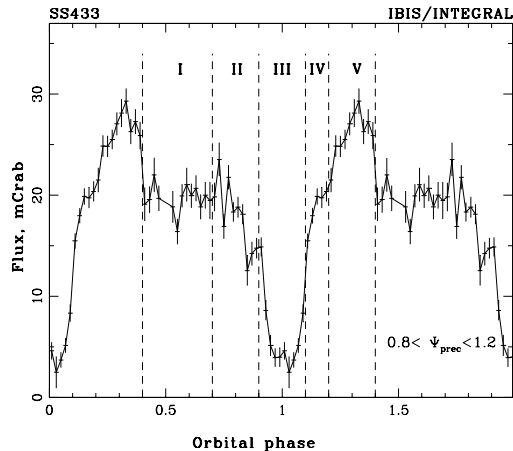


Figure 5. Binned X-ray light curve ($\Delta\phi_{orb} = 0.02$) with orbital phase intervals I-V for spectral analysis (vertical dashed lines).

is shown in Fig. 3. To plot this Figure, all available observations of SS433 by *INTEGRAL* with a total exposure time of about 8.5 Ms were used. The precession light curves were separately constructed for uneclipsed ($0.2 < \phi_{orb} < 0.8$) and middle-eclipse ($0.95 < \phi_{orb} < 1.05$) observations. Light curves in both bands show precessional variability and were used to constrain binary system parameters (see Cherepashchuk et al. (2009) and Section 5 below).

The hard X-ray precessional variability of the source has been found to be quite significant and stable over several precessional periods. The maximum to minimum flux ratio of the average precessional variability is around 5-7, which is higher than that in softer X-ray bands, and suggests the hard X-ray emission originating closer to the base of the visible part of the jets. The secondary maximum at the precessional phase ~ 0.6 is clearly seen in both 18-40 keV and 40-60 keV light curves (Fig. 3). The precessional 18-60 keV light curve constructed for data taken at the middle of X-ray eclipse (Fig. 2) has a non-zero flux at all precessional phases, as expected from a hot scattering corona above the accretion disk.

3.1 Orbital variability

The composite IBIS/ISGRI 18-60 keV light curve of the primary X-ray eclipse at precessional phase zero (sets I-VII from Table 1) is shown in Fig. 4. Data were analyzed using the IKI *INTEGRAL* data processing code described in Molkov et al. (2004). **The variable character of emission from SS433 is clearly seen in Fig. 4. For example, some**

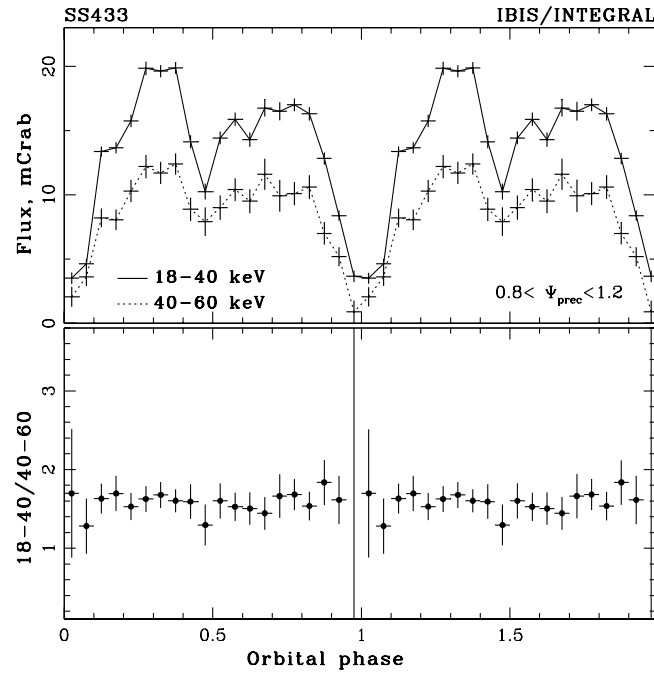


Figure 6. IBIS/ISGRI 18-40 and 40-60 keV orbital light curves (the upper and lower curves, respectively, on the upper panel) with the hardness ratio (bottom panel).

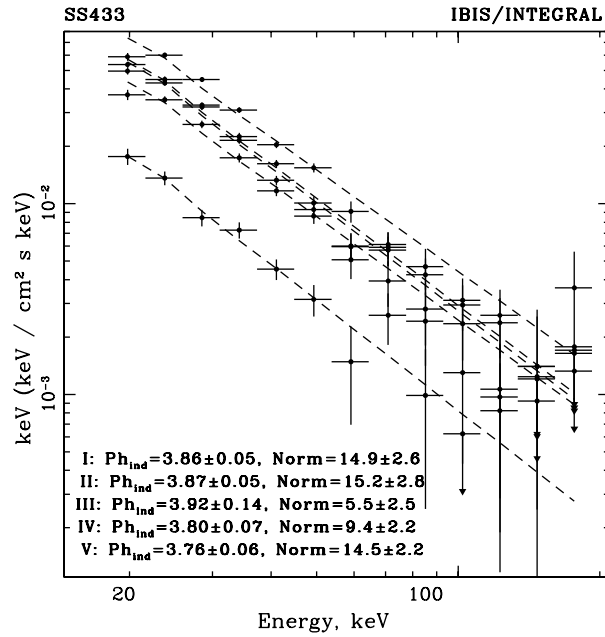


Figure 7. Phase-resolved IBIS/ISGRI spectra of SS433 within chosen orbital phase intervals I-V shown in Fig. 5. $1-\sigma$ errors are shown.

eclipses (e.g. in May 2007, shown in Fig. 1), are atypically broad, and we have not included them in our analysis. Fig. 4 clearly demonstrates that the eclipse ingress is more stable than the eclipse egress, and we specially stressed this point in previous publications (Cherepashchuk et al. 2009). The variability of eclipse egresses, likely reflecting the complex geometry of gas flows in SS433, makes the light curve modeling very difficult. However, the flux averaging within orbital phase bins $\Delta\phi_{orb} = 0.02$ increases the signal-to-noise ratio. The eclipse light curve averaged within orbital phase bins $\Delta\phi_{orb} = 0.02$ is shown in Fig. 5. 3σ -flux errors are indicated. The 18-40 and 40-60 keV orbital light curves with the corresponding hardness ratios are presented in Fig. 6. **Figs. 5 and 6 show that the averaged eclipse light curve of SS433 demonstrates regular features at orbital phases ~ 0.2 and ~ 0.7 , which we will discuss in the next Section.**

Earlier we have shown (Cherepashchuk et al. 2009) that the form of hard X-ray spectrum of SS433 does not change with the precessional phase: at maximum and minimum of the precessional variability, the spectrum is fitted by a power-law $dN/dE/dt/dA \sim E^{-\Gamma_{ph}}$ with the photon index $\Gamma_{ph} \approx 3.8$. The accumulated by the present time *INTEGRAL* data allowed us to make, for the first time, the *orbital phase-resolved X-ray spectroscopy*. Five orbital phase intervals chosen for spectral analysis are shown by the vertical dashed lines in Fig. 5. The obtained X-ray spectra within each orbital phase intervals I-V are shown in Fig. 7. It is seen that within errors they have an identical power-law shape with the same photon spectral index $\Gamma_{ph} \simeq 3.8$. Nevertheless, there is a tendency of the spectrum to get harder at $\phi_{orb} \sim 0.25$ (phase interval V in Fig. 5) than at $\phi_{orb} \sim 0.75$ (phase interval I in Fig. 5). Note also that at the middle of the eclipse (phase interval III in Fig. 5) the spectrum gets softer. This is exactly what is expected in the jet nutation picture: during the disk-jet nutation the angle between the line of sight and the jet axis changes by ~ 6 degrees, so the observer looks into the funnel less (at $\phi_{orb} = 0.5$) or more (at $\phi_{orb} = 0.75$) deeper, thus observing cooler or hotter parts of the jet base, respectively (see Section 4 below for more detail). **The X-ray spectral variations across the orbital eclipse can provide insight into the nature and structure of the hard X-ray emission region (see, for example, discussion in Filippova et al. (2006) and Krivosheyev et al. (2009)). Therefore, observations with higher sensitivity are required to confirm or dismiss the spectral variations.**

4 NUTATIONAL VARIABILITY

From theoretical point of view, short-term motions in precessing accretion disks in close binary systems occur when the binary orbital period is not negligible compared with the precession period. This is the case of SS 433. Theoretical analysis predicts a $6^d.3$ periodic component of the moving spectral lines of SS 433 at an amplitude of $\sim 10\%$ of the 164^d precessional motion (Katz et al. 1982; Levine & Jernigan 1982; Collins & Newsom 1986), this prediction is in a very good agreement with observations. Studies by Katz et al. (1982); Levine & Jernigan (1982); Collins & Newsom (1986) show that the nutational motion in SS433 can be understood in terms of the forced (slaved) disc precession (van den Heuvel et al. 1980; Whitmire & Matese 1980).

Nutational variability in SS433 (nodding motion of tilted accretion disk) has been observed in the optical (Goranskij et al. 1998; Davydov et al. 2008) and radio (Trushkin et al. 2001) bands. At the time of the maximum disk opening (precessional phase zero, moment T3), the node line of the disk is normal to the line of sight, and the nutational variability must be observed as a wobbling of the disk inclination angle to the line of sight with the nutational period $P_{nut} \approx 6.29$ days (Katz et al. 1982; Levine & Jernigan 1982). The analysis of an almost 30-years long optical spectroscopy of SS433 carried out by Davydov et al. (2008) gives the ephemeris for the nutational motion of jets (the time when the H_α emission lines from jets are most widely separated)

$$t_{max} = \text{JD}2443009.720271 + (6^d.287599 \pm 0^d.00035) \times E.$$

A significant flux excess at the orbital phase $\phi_{orb} \sim 0.25$ in the composite 18-60 keV *INTEGRAL* light curve (Fig. 4 and 5) is observed after the primary eclipse relative to the phase 0.75 before the eclipse. On the 40-60 keV light curve (Fig. 6) two maxima with similar amplitude are clearly seen at both orbital phases 0.25 and 0.75. These $\sim 10\%$ sine-like variability occurring at about twice the orbital period, superimposed on the orbital light curve of SS433, is most likely due to the jet nutation. The effect must be maximal at precessional phase zero when the binary system is observed in quadratures (i.e. at the binary phases 0.25 and 0.75). Due to nutation, the jet changes its inclination angle to the line of sight by $\delta\epsilon \approx 6^\circ$. Thus, the composite *INTEGRAL* light curve allowed us to see for the first time the jet nutation in the 40-60 keV band (Cherepashchuk et al. 2012).

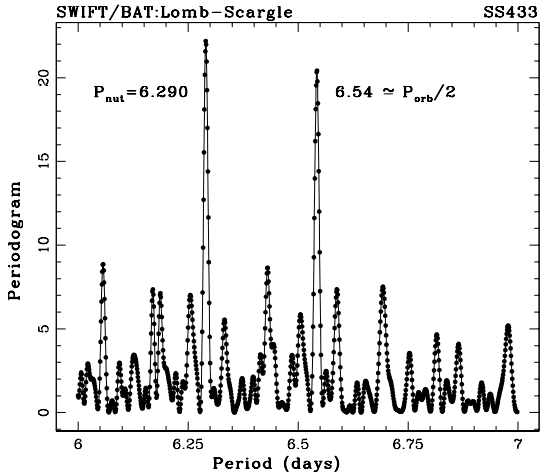


Figure 8. The Lomb-Scargle periodogram constructed for *Swift/BAT* 15-50 keV observations of SS433 at precessional phases $0.8 < \psi_{pr} < 1.2$. The peaks at about half orbital period $6^{\text{d}}.54$ and nutation period $6^{\text{d}}.290$ are indicated.

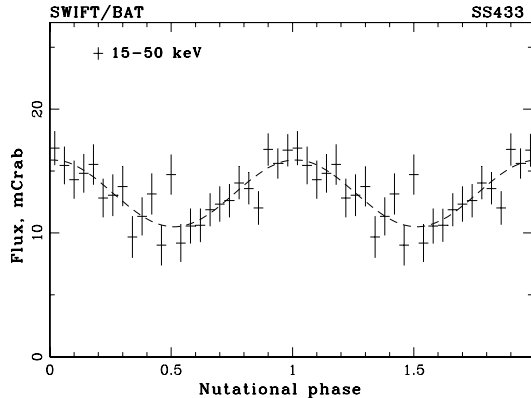


Figure 9. Off-eclipse *Swift/BAT* 15-50 keV nutation light curve of SS433. The dashed curve shows a sine-line best-fit to the data.

4.1 Nutational variability of SS433 from *Swift/BAT* monitoring

To substantiate this result, we first have performed the frequency analysis of the public archival data obtained with the Burst Alert Telescope (BAT, 15-150 keV, Barthelmy et al. 2005) onboard the Swift observatory (Gehrels et al. 2004). For this purpose, we have used the 15-50 keV data seen only at precessional phases $0.8 < \psi_{pr} < 1.2$ (i.e. around moment T3). The Lomb-Scargle periodogram (Lomb 1976; Scargle 1982) is shown in Fig. 8. The prominent peaks at about half orbital period $6^{\text{d}}.54$ and the nutation period $6^{\text{d}}.290$ are clearly seen. **Their amplitudes imply a chance probability of less than 10^{-4} (Baluev 2008).** Note that the value of the nutation period from the *Swift/BAT* data agrees, within the errors, with that derived from the optical data (Davydov et al. 2008). The *Swift/BAT* nutational light curve (only for observations near moments T3 $0.8 < \psi_{pr} < 1.2$ and off-eclipse with $0.8 < \phi_{orb} < 1.2$), convolved with the $P_{nut} = 6^{\text{d}}.290$ period, is presented in Fig. 9. **The folded *Swift/BAT* lightcurve is not consistent with a constant: the fit by a constant yields $\chi^2 \approx 61$ for 25 d.o.f. Adding a sine component with period $6^{\text{d}}.290$ d strongly improves the fit, giving $\chi^2 \approx 20$ for 24 d.o.f. We conclude that the sine line with amplitude $\Delta F_{nut} = 2.7 \pm 0.5$ mCrab plus constant component $F_0 = 13.2 \pm 0.4$ mCrab (the dashed line in Fig. 9) adequately describes the data.** The relative *Swift/BAT* nutational variability is $\Delta F_{nut}/F_0 \approx 0.205$.

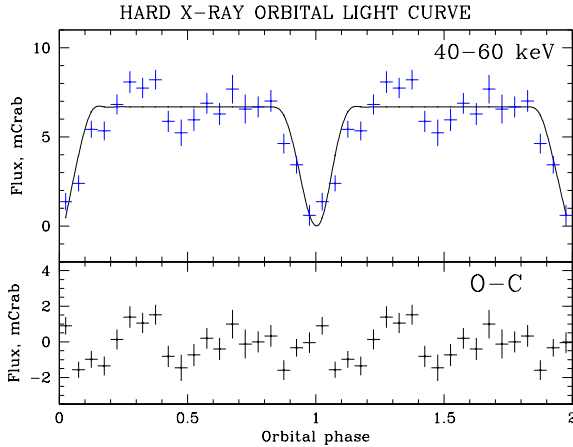


Figure 10. 40-60 keV light curve fitted with the geometrical model of the primary eclipse for $q = 0.3$ (upper panel) and the residuals (bottom panel).

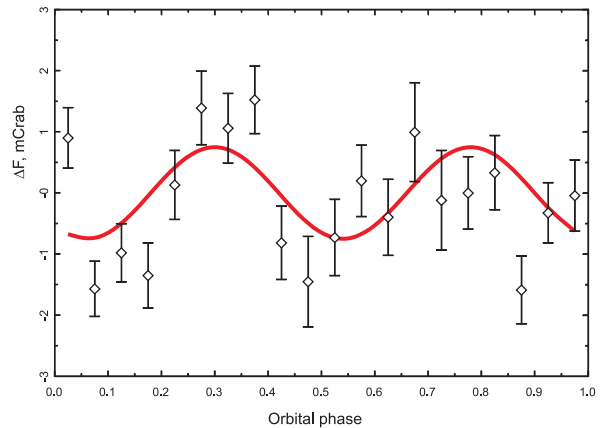


Figure 11. Residuals of the 40-60 keV orbital light curve fitted with nutational variability of SS433 (equation (1)).

4.2 Fitting nutational variability in the *INTEGRAL* orbital light curve

Following Katz et al. (1982); Levine & Jernigan (1982); Collins & Newsom (1986) we parametrize the change in the observed flux ΔF due to the nutational motion of the disk and jets as follows:

$$\Delta F_{nut} = A \sin(\omega_{nut}t + c_0) = a \sin(2\pi(\varphi_{orb} + \varphi_0)P_{orb}/P_{nut}), \quad (1)$$

where A is the amplitude, $\omega_{nut} = 2\pi/P_{nut}$ is the nutational angular velocity, t is the time, c_0 is a constant, $\varphi_{orb} = t/P_{orb}$ is the orbital phase, φ_0 is the phase angle between the orbital and the nutational minima, P_{orb} is the orbital period of the system, P_{nut} is the period of nutation. The ratio $P_{orb}/P_{nut} = 2.08$ is fixed, while A and φ_0 are free parameters (see e.g. Katz et al. (1982), equation [20]). The third mode of nutational variability is the dominant $6^d.3$ mode, its angular velocity is $\omega_{nut} = 2\dot{\eta} - \Omega_s$, where η is the orbital frequency of the companion star, Ω_s is the mean precessional rate of the accretion ring. We neglect the term $0.5\dot{\Omega}t^2$ in those equation, because all our data are averaged over one orbital period.

We have performed an independent analysis of the nutational variability in the *INTEGRAL* 40-60 keV data. To this aim, we have subtracted the best-fit geometrical primary eclipse light curve calculated for the binary mass ratio $q = 0.3$ (see Section 5 for more detail) (Fig. 10, the solid curve on the upper panel). The residual light curve (points with error bars in Fig. 11) has been fitted with a sine curve (1) (the solid line in Fig. 11) with parameters $A = 0.75$ mCrab, $\varphi_0 = 0.30$. The value of χ^2 -test for this fit is $\chi^2 = 47.63$ for 18 d.o.f., giving the reduced $\chi^2_{dof} \approx 2.65$. With such an amplitude and $F_0 \approx 7$ mCrab (see Fig. 10),

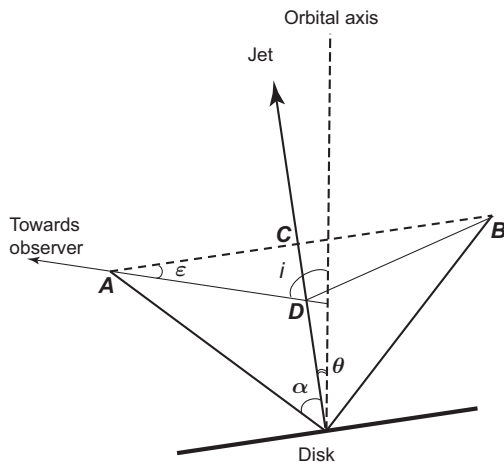


Figure 12. Scheme of nutation angles in SS433. Binary inclination angle is $i = 79^\circ$, jet inclination angle to the orbital angular momentum is $\theta = 20^\circ$, jet funnel opening half-angle is $\alpha < (i - \theta)$.

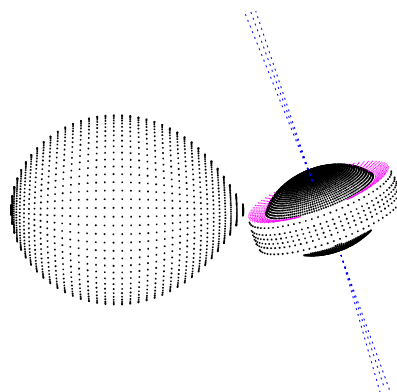


Figure 13. Model view of SS433 for binary mass ratio $q = 0.3$ is shown at the disk precession angle 80 degrees. Thin jets normal to the disk plane are shown, but their contribution to hard X-ray emission is ignored.

the fractional 40-60 keV flux change due to the nutational motion is $\Delta F_{nut}/F_0 \approx 0.11$, which is smaller but consistent, within errors, with the *Swift*/*BAT* amplitude ≈ 0.205 . The larger value of $\chi_{dof}^2 \approx 2.65$ for *INTEGRAL* data in comparison with *Swift*/*BAT* nutational light curve fitting ($\chi_{dof}^2 \approx 1$) is due to our using, in this Section, data folded with the orbital period of SS433; as $P_{orb}/2$ and P_{nut} are slightly different, the dispersion of points around the mean nutational light curve in the *INTEGRAL* data are larger than for the *Swift*/*BAT* data.

4.3 Geometrical model of nutational variability in SS433

The relative nutational flux variability 10–15% can be explained in the frame of the simplest geometrical model of nodding funnel around jets filled with hot scattering plasma. Let the line of sight make an angle ϵ with the jet normal, as sketched in Fig. 12. From the kinematical model of SS433 (Margon 1984) we adopt the binary inclination angle to be $i \approx 79^\circ$, the jet precession angle to be $\theta \approx 20^\circ$, and the jet nutation angle to be $\delta\theta \approx 6^\circ$. We also assume the opening angle of the jet funnel α . From the geometry (Fig. 12) we find $\epsilon = \pi/2 - i + \theta$. If $\alpha < i - \theta = 59^\circ$ (which is supported by numerical simulations of wind from supercritical accretion disk in SS433, see e.g. Okuda et al. (2009)), then the relative change in the volume of the jet funnel filled with hot scattering plasma seen by the observer due to jet nutation is

$$\frac{\delta V}{V} = \frac{\delta CD}{CD} = \frac{\delta \tan \epsilon}{\tan \epsilon} = \frac{\delta \theta}{\cos(i - \theta) \sin(i - \theta)} \approx 0.23$$

(here the observed volume is approximated by the cone ABD in Fig. 12; the closer the jet funnel angle α to $(i-\theta)$, the better this approximation). Therefore, in the first approximation, the relative change in the hard X-ray flux from this volume in one nutational period is $\delta F/F = \delta V/V \approx 0.23$, which is somewhat larger than the observed value $0.11 \div 0.20$ obtained in our analysis of the *INTEGRAL* and *Swift/BAT* data. However, in view of roughness of the simple geometrical model, we can conclude that the observed relative amplitude of the nutational variability is in agreement with the geometry of jets and accretion funnel in SS433.

5 PARAMETERS OF SS433 FROM ANALYSIS OF HARD X-RAY LIGHT CURVES

5.1 Broadband 18-60 keV orbital light curve

The *INTEGRAL* observations of SS433 provide three different light curves, which can be used to constrain the parameters of the system: 1) the orbital light curve, 2) the precessional light curve out of eclipses, and 3) precessional light curve in the middle of the eclipses (see Fig. 14, upper panels, and lower panels). We use a geometrical model described in detail in Antokhina et al. (1992); Cherepashchuk et al. (2009). Briefly, the model includes an optical star with mass M_v filling its Roche lobe, a compact star with mass M_x surrounded by an optically thick accretion disk with radius a_d , and a hot corona which is modeled as a broad 'jet' parametrized by the part of ellipse with semi-axes a_j and b_j normalized to the binary orbital separation. The elliptical corona is restricted by the cone with half-angle α (see Fig. 13). The shape and amplitude of the precessional light curve constrain the height of the hot X-ray corona, while the orbital light curve restricts the accretion disk radius. At a given binary mass ratio, after finding the best parameters for the precessional variability, we can calculate the deviations of the model orbital light curve from the observed one. The results of the joint analysis of the orbital and precessional 18-60 keV light curves of SS433 are shown in Fig. 14. In the present analysis, we neglected the contribution of thermal X-ray emission from jets.

The new *INTEGRAL* data added after 2008 fully confirm the results of our analysis published in Cherepashchuk et al. (2009). While the eclipsing light curve alone can be well reproduced by a small mass ratio $q = m_x/m_v \sim 0.1$ in the model with 'long' X-ray emitting jet ($b_j > 0.5$), the observed precessional light

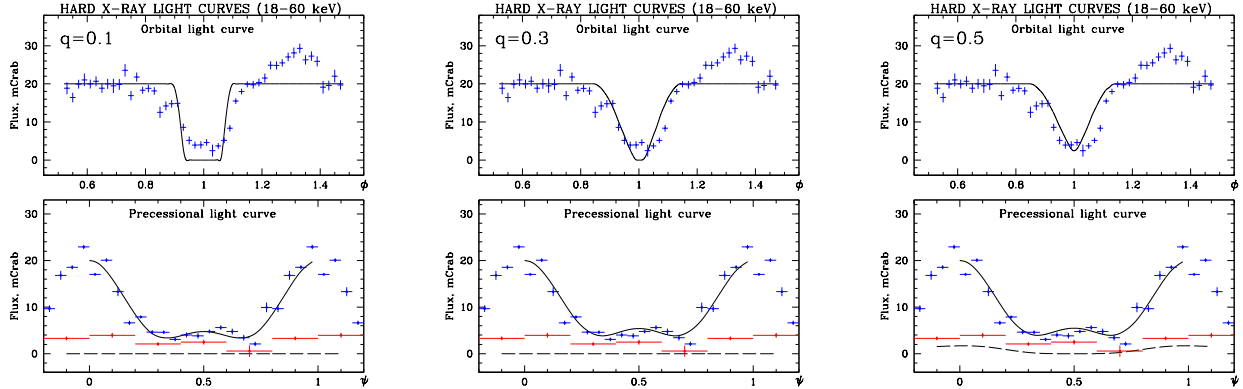


Figure 14. Joint analysis of orbital (upper plots) and precessional (lower plots) 18-60 keV light curves of SS433. On the upper plots, the model orbital light curve is shown by the solid line. On the bottom panels, the model precessional light curves off eclipses ($0.2 < \phi_{orb} < 0.8$) and in eclipses ($0.95 < \phi_{orb} < 1.05$) are shown by the solid and dashed lines, respectively. The observed precessional variability in the middle of eclipse are shown by the gray (red in color on-line version) crosses. Left panel: $q = 0.1$, 'short jet' corona ($a_j = 0.25$, $b_j = 0.1$, $\alpha = 40^\circ$). Middle panel: $q = 0.3$, 'short jet' corona ($a_j = 0.35$, $b_j = 0.13$, $\alpha = 80^\circ$). Right panel: $q = 0.5$, 'short jet' corona ($a_j = 0.35$, $b_j = 0.13$, $\alpha = 80^\circ$).

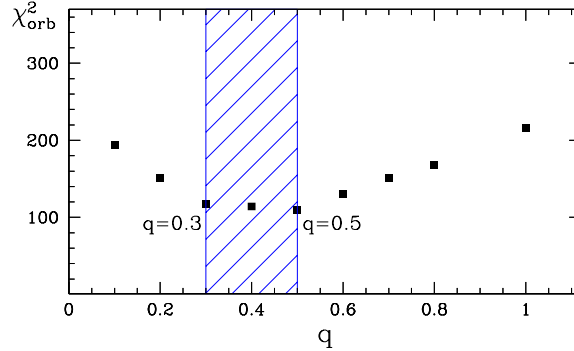


Figure 15. χ^2 -value for the orbital light curve (18-60 keV) for different binary mass ratios q .

curve cannot be reproduced by models with small binary mass ratios $q \leq 0.25$ (see Fig. 16a below). Models with 'short' X-ray emitting jet ($b_j \sim 0.1 \div 0.2$) and small mass ratio $q = 0.1$ can fit the observed precessional variability, but fail in describing the X-ray primary eclipse form (see Fig. 14a).

In Fig. 15 we plot the values of χ^2 for orbital 18-60 keV light curve of SS433 shown in upper panels of Fig. 14 as a function of the binary mass ratio q (i.e. with the disk and coronal 'jet' parameters which fit the precessional light curve as shown in lower panels of Fig. 14). It is seen that within the interval $0.3 < q < 0.5$ the model fits yield similar χ^2 values. This mass ratio range is consistent with results of an independent analysis of the orbital and precessional variability of SS433 in the optical (Antokhina & Cherepashchuk 1987).

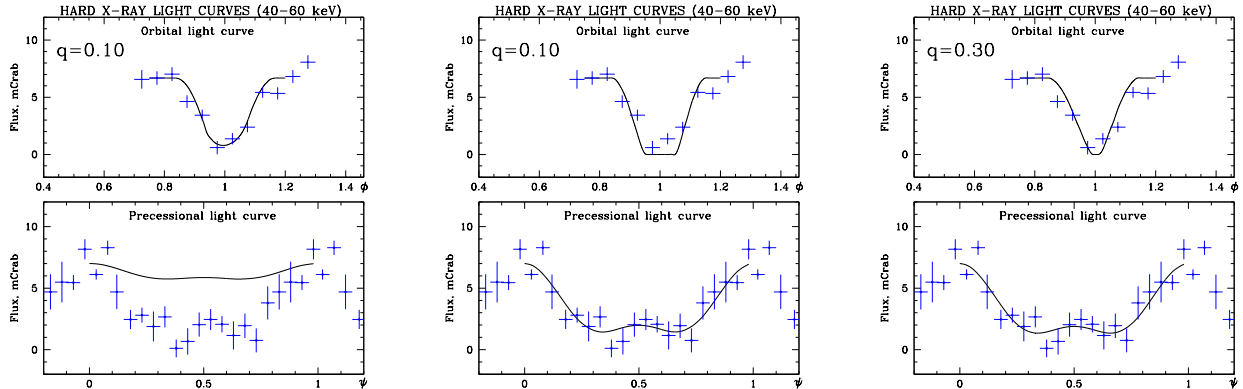


Figure 16. Joint analysis of orbital (upper plots) and precessional (lower plots) 40-60 keV IBIS/ISGRI light curves of SS433. Left panel: $q = 0.1$, 'long jet' corona ($a_j = 0.25$, $b_j = 0.55$, $\alpha = 80^\circ$); only orbital light curve can be reproduced. Middle panel: $q = 0.1$, 'short jet' corona ($a_j = 0.25$, $b_j = 0.1$, $\alpha = 80^\circ$). Both orbital and precessional light curves can be fitted, but the total eclipse (plateau at zero flux) appears (unobserved). Right panel: $q = 0.3$, 'short jet' corona ($a_j = 0.35$, $b_j = 0.13$, $\alpha = 80^\circ$); both orbital and precessional light curves are well reproduced.

5.2 Hard X-ray (40-60 keV) orbital light curve

To avoid contamination from thermal X-ray emission from relativistic jets, we repeated the analysis using only hard X-ray 40-60 keV light curves shown in Fig. 3 and Fig. 6. The result for different mass ratios $q = M_x/M_v$ is presented in Fig. 16. It is seen that the hard X-ray orbital and precessional light curves can be simultaneously reproduced by the geometrical model for the binary mass ratio $q \gtrsim 0.3$ (at smaller mass ratios a plateau corresponding to the total eclipse of the hot corona by the optical star appears in the orbital light curve, which is not observed), in agreement with the analysis of the broadband 18-60 keV orbital and precessional light curves shown in Fig. 14.

6 DISCUSSION

The analysis of all *INTEGRAL* observations of SS433 in 2003-2011 confirms our earlier conclusions about binary system parameters (Cherepashchuk et al. 2009). With the obtained range of the binary mass ratio $q = 0.3 \div 0.5$, there are three possible ways to estimate the mass of the compact star m_x in SS433.

(i) Using optical spectroscopy of the optical component A7I in the range $4400 \div 5000$ Å, Hillwig et al. (2004) and Hillwig & Gies (2008) measured the semiamplitude of the radial velocity curve of the mass donor star of 58.2 ± 3.1 km s⁻¹, yielding the optical star mass function

$$f_v(m) = \frac{m_x \sin^3 i}{(1 + 1/q)^2} \simeq 0.268 M_\odot, \quad (2)$$

For $q = 0.3 \div 0.5$, from this mass function we obtain masses of the compact object and the optical star $m_x \simeq 5.3M_\odot \div 2.6M_\odot$ and $m_v \simeq 17.7M_\odot \div 5.1M_\odot$, respectively.

(ii) From the optical spectroscopy of the accretion disk emission lines (Crampton & Hutchings 1981; Fabrika & Bychkova 1990) (using He II 4686 Å emission line) and Gies et al. (2002a) (using CII 7231, 7236 Å emission lines) derived the semiamplitude for the compact star radial velocity 195 km s⁻¹ (Crampton & Hutchings 1981), 175 km s⁻¹ (Fabrika & Bychkova 1990), 162 km s⁻¹ (Gies et al. 2002a). The average value of the compact star mass function for the last two compact star radial velocity estimates is

$$f_x(m) = \frac{m_v \sin^3 i}{(1 + q)^2} \simeq 6.4M_\odot, \quad (3)$$

For $q = 0.3 \div 0.5$ and the orbital inclination angle $i \simeq 78.8^\circ$ (Margon & Anderson 1989), this yields masses of the compact object and the optical star in SS433 $m_x \simeq 3.44M_\odot \div 7.63M_\odot$, $m_v \simeq 11.46M_\odot \div 15.26M_\odot$, respectively.

(iii) From the high-resolution optical spectroscopy of circumbinary shell of SS433 Blundell et al. (2008) and Bowler (2013) estimated the total mass of SS433 binary system to be $m_x + m_v \gtrsim 40M_\odot$. For $q = 0.3 \div 0.5$ this gives the lower limits of the masses of the components in SS433: $m_x \gtrsim 9.23M_\odot \div 13.33M_\odot$, $m_v \gtrsim 30.77M_\odot \div 26.67M_\odot$. **The compact object mass derived from these observations is about twice as high as from radial velocity measurements.**

Therefore, three independent estimates of the compact star mass in SS433 (higher than $\approx 2.6 \div 3M_\odot$) suggest it to be a black hole. However, for accurate determination of the mass of the compact star, further high-resolution spectroscopic observations of SS433 are highly desirable to improve estimates of the spectral class and radial velocity curve of the optical star. It is also important to improve the radial velocity curve from observations of emission lines (He II 4686, CII 7231,7236, etc.) in order to reliably determine the mass function of the compact star.

7 CONCLUSIONS

1) *INTEGRAL* observations of SS433 in hard X-rays 18-60 keV allowed us for the first time to make orbital-resolved spectroscopy of the X-ray eclipse in the precessional phase corresponding to the maximum opening angle of the disk. The hard X-ray continuum is fitted with a power-law with photon index $\Gamma \approx 3.8$ which does not significantly change

across the eclipse, suggesting the origin of this emission as being due to scattering in hot corona surrounding the funnel around the jets in a supercritical accretion disk in SS433.

2) For the first time, *INTEGRAL* observations of SS433 revealed the presence of the secondary maximum in the hard X-ray precession light curve of the source at the precessional phase $\psi_{pr} \approx 0.6$ of the relative amplitude ~ 2 (with a total relative amplitude of the precessional variability of 5-7). The secondary maximum is seen in both broad-band 18-60 keV and hardest 40-60 keV bands.

3) For the first time, the joint analysis of hard X-ray (40-60 keV) orbital and precessional light curves has been performed. This analysis independently confirms our previous result (Cherepashchuk et al. 2009) that the low value of the mass ratio $q = M_x/M_v$ in SS433 cannot reproduce the observed orbital and precessional light curves. With the existing estimates of the mass function of the optical and compact star, the **obtained binary mass ratio range** $q \sim 0.3 \div 0.5$ points to the black hole nature of the compact star in SS433. The black-hole mass of the compact star is found from three independent measurements.

4) The shape of the hard X-ray orbital light curve 18-60 keV demonstrates two humps at around orbital phases 0.25 and 0.75, most likely due to the nutation effects in SS433. These humps are mostly pronounced in the 40-60 keV orbital light curve. The nutation effect in SS433 with a period of $P_{nut} \simeq 6^d.290$ with similar relative amplitude is independently confirmed by the analysis of *Swift/BAT* observations of SS433.

New *INTEGRAL* observations of SS433 at different precessional phases will be used to further constrain physical parameters of this unique galactic microquasar.

ACKNOWLEDGMENTS

We thank the anonymous referee for critical reading of the manuscript and useful notes which allowed us to improve the paper. The results of this work are based on observations with *INTEGRAL*, an ESA project with instruments and science data centre funded by ESA member states (especially the PI countries: Denmark, France, Germany, Italy, Switzerland, Spain), and Poland, and with the participation of Russia and the USA. The data were obtained from the European and Russian *INTEGRAL* Science Data Centers^{1,2}. The work of AMCh, EAA

¹ <http://isdc.unige.ch>

² <http://hea.iki.rssi.ru/rsdc>

and AIB was partially supported by the RFBR grant 11-02-00258 and by the Program for State Support of Leading Scientific Schools of RF 2374.2012.2. SVM was partially supported by RFBR grant 11-02-01328 and the Ministry of Education and Science of RF through Contract N8701. KAP was partially supported by RFBR grant 12-02-00186.

REFERENCES

- Antokhina E.A., Cherepashchuk A.M., 1987, SvA, 31, 295
- Antokhina E.A., Seifina E.V., Cherepashchuk A.M., 1992, SvA, 36, 143
- Baluev R.V., 2008, MNRAS, 385, 1279
- Barthelmy S.D. et al., 2005, Space Sci. Rev., 120, 143
- Begelman M.C., King A.R., Pringle J.E., 2006, MNRAS, 370, 399
- Blundell K. M., Bowler M. G., Schmidtobreick L., 2008, ApJ, 678, L47
- Bowler M. G., 2013, A&A, 556, A149
- Brinkman W., Kawai N., Matsuoka M., 1989, A&A, 218, L13
- Burenin R.A., Revnivtsev M.G., Khamitov I.M., 2011, Astron. Letters, 37, 100
- Cherepashchuk A.M., 1981, MNRAS, 194, 761
- Cherepashchuk A.M., 1989, Sov. Sci. Rev. Ap. Space Phys., Ed. by R.A.Sunyaev, v.7, p.185
- Cherepashchuk A.M., Bychkov K.V., Seifina E.V., 1995, ApSS, 229, 33
- Cherepashchuk A.M., Sunyaev R.A., Seifina E.V., Panchenko I.E., Molkov S.V., Postnov K.A., 2003, A&A, 411, L441
- Cherepashchuk A.M. et al, 2005, A&A, 437, 561
- Cherepashchuk A.M. et al, 2007, Proc. 6th *INTEGRAL* Workshop, ESA SP-622, p. 319
- Cherepashchuk A.M., Sunyaev R.A., Postnov K.A., Antokhina E.A., Molkov S.V., 2009, MNRAS, 397, 479
- Cherepashchuk A., Sunyaev R., Molkov S., Antokhina E., Postnov K., Bogomazov A., 2013, in Proc. 9th *INTEGRAL* Workshop, PoS(*INTEGRAL* 2012), id.40 (arXiv:1212.3443)
- Collins II G. W., Newsom G. H., ApJ, 1986, 308, 144
- Crampton D., Hutchings J. B., ApJ, 1981, 251, 604
- Davydov V.V., Esipov V.F., Cherepashchuk A.M., 2008, Astron. Rep., 52, 487
- Fabrika, S.N., 2004, Astrophys. Space Phys. Rev., 12, 1
- Fabrika S. N., Bychkova L. V., 1990, A&A, 240, L5

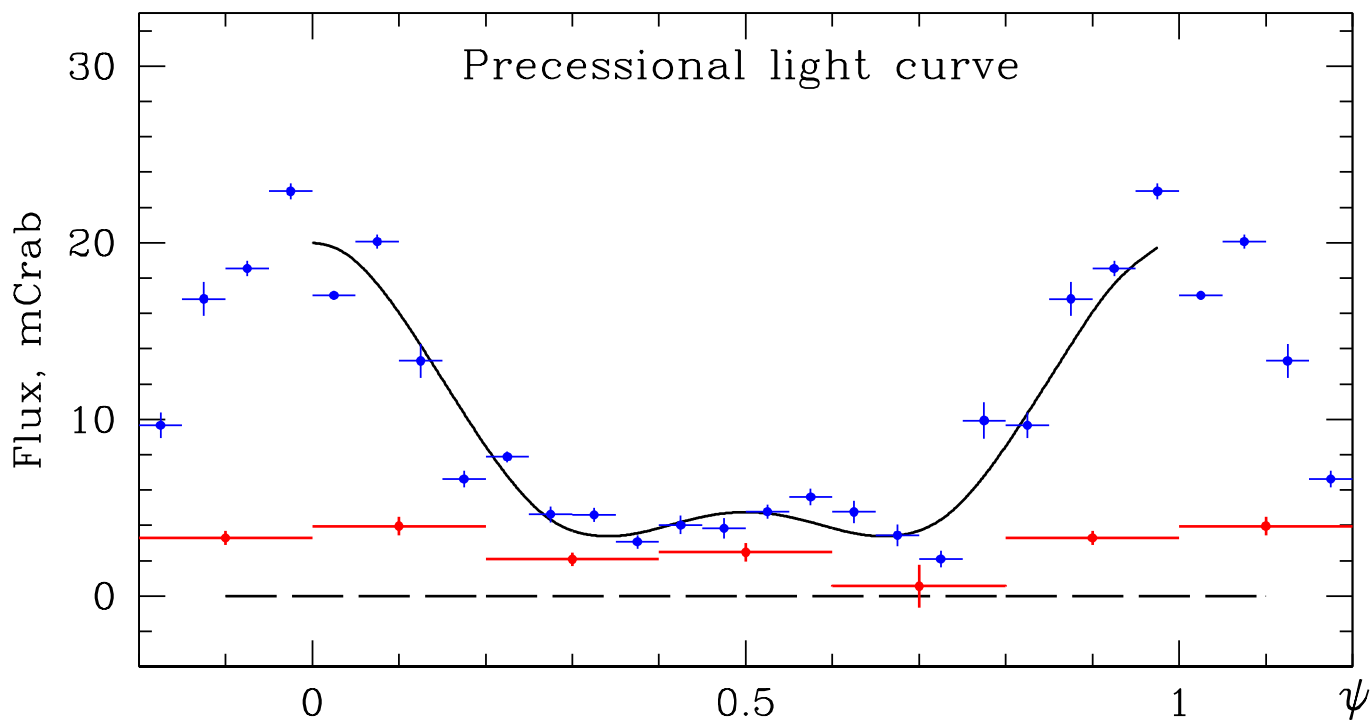
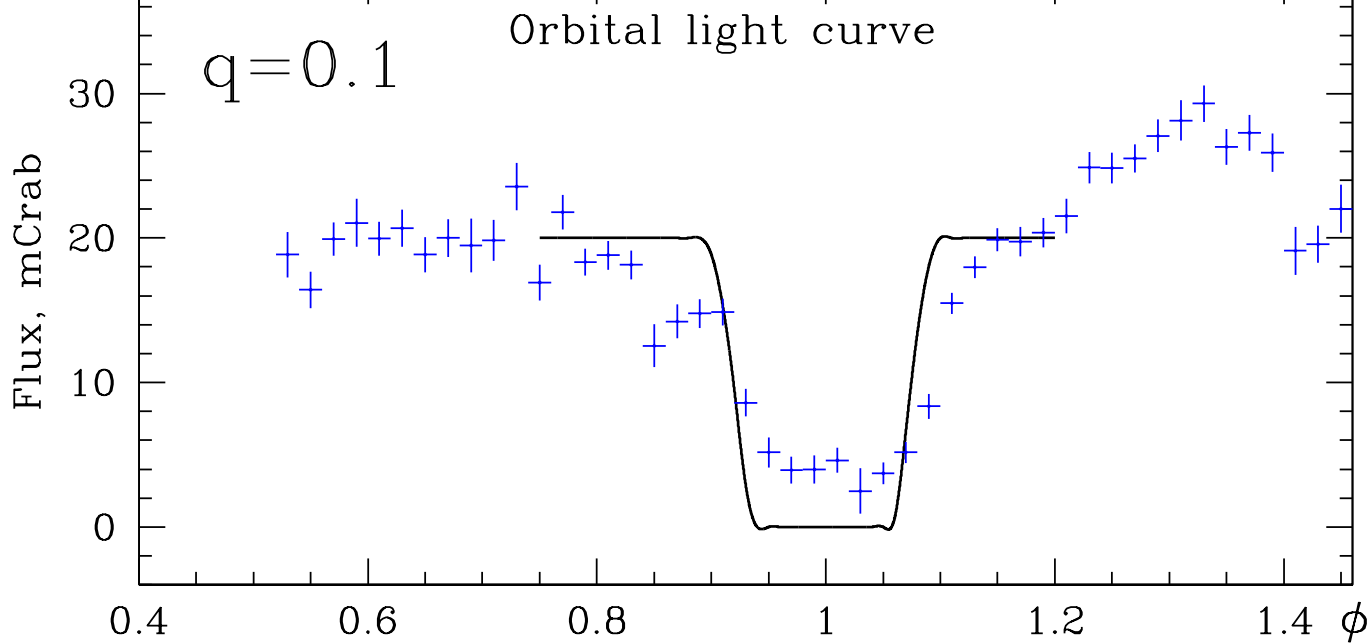
- Filippova E., Revnivitsev M., Fabrika S., Postnov K., Seifina E., 2006, *A&A*, 460, 125
- Gehrels N. et al., 2004, *ApJ*, 611, 1005
- Gies D.R. McSwain M.V., Riddle R.L., Wang Z., Wiita P.J., Wingert D.W., 2002a, *ApJ*, 566, 1069
- Gies D.R., Huang W., McSwain M.V., 2002b, *ApJ*, 578, L67
- Goranskij V.P., 2011, *Peremennye Zvezdy*, 31, N5 [arXiv:1110.5304]
- Goranskij V.P., Esipov V.F., Cherepashchuk A.M., 1998, *Astron. Rep.*, 42, 209; *ibid.*, p. 336
- Hillwig T.C., Gies D.R., Huang W., McSwain M.V., Stark M.A., van der Meer A., Kaper L., 2004, *ApJ*, 615, 422
- Hillwig T.C., Gies D.R., 2008, *ApJ*, 676, L37
- Katz J.I., Anderson S.F., Grandi S.A., Margon B., 1982, *ApJ*, 260, 780
- Kawai N., Matsuoka M., Pan H.-C., Stewart G.C., 1989, *PASJ*, 41, 491
- Kotani T., 1998, PhD. The Institute of Space and Astronautical Science. Japan
- Kotani T., Kawai N., Matsuoka M., Brinkmann W., 1998, in *Proc. IAU Symp. 188*, eds. K. Koyama, S. Kitamoto, M. Itoh, Dordrecht: Kluwer, p. 358
- Krivosos R., Revnivitsev M., Tsygankov S., Sazonov S., Vikhlinin A., Pavlinsky M., Churazov E., Sunyaev R., 2010, *A&A*, 519, A107
- Krivosheyev Yu. M., Bisnovatyi-Kogan G.S., Cherepashchuk A.M., Postnov K.A., 2009, *MNRAS*, 394, 1674
- Levine A.M., Jernigan J.G., 1982, *ApJ*, 262, 294
- Lomb N.R., 1976, *ApSS*, 39, 447
- Margon B., 1984, *ARA&A*, 22, 507
- Margon B., Anderson S.F., 1989, *ApJ*, 347, 507
- Molkov S., Cherepashchuk A.M., Lutovinov A.A., Revnivitsev M.G., Postnov K.A., Sunyaev R.A., 2004, *Astron. Lett.*, 30, 534
- Namiki M., Kawai N., Kotani T., Makishima K., 2003, *PASJ*, 55, 281
- Okuda T., Lipunova G.V., Molteni D., 2009, *MNRAS*, 398, 1668
- Revnivitsev M. et al., 2004a, *A&A*, 424, L5
- Revnivitsev M.G. et al., 2004b, *Astron. Lett.*, 30, 382
- Revnivitsev M. et al., 2006, *A&A*, 447, 545
- Scargle J., 1982, *ApJ*, 263, 835
- Shakura N.I., Sunyaev R.A., 1973, *A&A*, 24, 337

Trushkin S.A., Borisov N.N., Smirnova Yu.V., 2001, *Ast. Rep.*, 45, 804

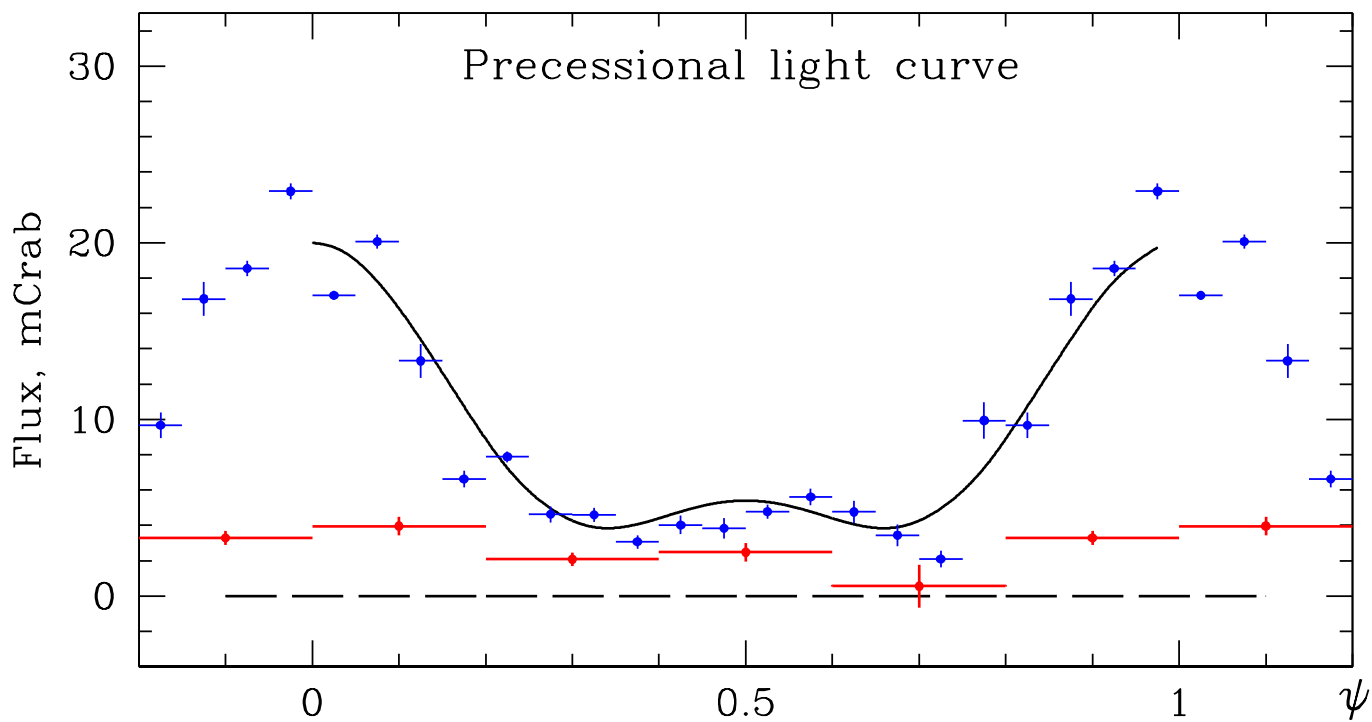
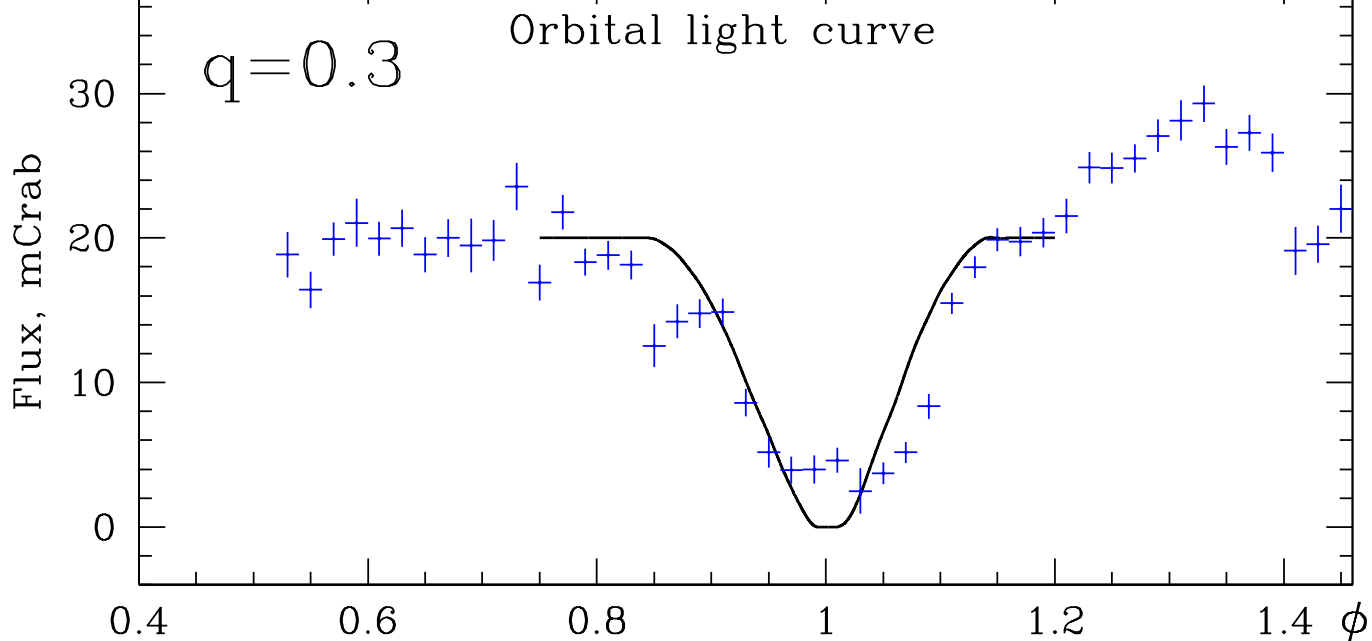
van den Heuvel E. P. J., Ostriker J. P., Petterson J. A., 1980, *A&A*, 1980, 81, L7

Whitmire D. P., Matese J. J., 1980, *MNRAS*, 193, 707

HARD X-RAY LIGHT CURVES (18–60 keV)



HARD X-RAY LIGHT CURVES (18–60 keV)



HARD X-RAY LIGHT CURVES (18–60 keV)

